

Comparison of the Effects of 3D Printing Bioactive Porous Titanium Alloy Scaffolds and Nano-biology for Direct Treatment of Bone Defects

Fei Wang^{1,2}, Jun Liu¹, Jincheng Liu¹, Sheng Zhang², Mingzhi Yang², Kai Kang^{1*}

¹Department of Orthopedics, Yanan University Affiliated Hospital, Yan'an 716000, China

²Department of Orthopedics, Yan'an People's Hospital, Yan'an 716000, China

ARTICLE INFO

Original paper

Article history:

Received: November 02, 2021

Accepted: March 16, 2022

Published: March 31, 2022

Keywords:

three-dimensional (3D) printed bioactive porous titanium alloy scaffolds, rhBMP-2/PLA sustained-release nanospheres, bone defects, femoral condyle defect model, treatment effect

ABSTRACT

This study was to compare the effects of three-dimensional (3D) printed bioactive porous titanium alloy scaffolds (3DP-BPTAS) and rhBMP-2/PLA-loaded sustained-release nanospheres (SRNs) in the treatment of bone defects. In this study, the bioactive porous titanium alloy scaffolds (BPTAS) with different pore sizes were prepared by selective laser melting (SLM) technology. The rhBMP-2/PLA SRNs were prepared by the double emulsion solvent volatilization method. The morphology of the two nanomaterials was observed under a scanning electron microscope (SEM). The encapsulation rate (ER), drug loading (DL), and *in vitro* release rate of the SRNs were detected by enzyme-linked immunosorbent assay (ELISA); and the effects of different particle sizes of BPTAS and SRNs on the proliferation of BMSCs were measured using the Methyl Thiazolyl Tetrazolium (MTT) method. 42 healthy male rabbits were selected and rolled into a control group (no treatment), a model group (the femoral condyle defect model), an A800 group (model + 800 μm of BPTAS), and an A1000 group (model + 1000 μm of BPTAS), an A1200 group (model + 1200 μm of BPTAS), an A1500 group (model + 1500 μm of BPTAS), and an SNR group (model + rhBMP-2/PLA SRNs). There were 6 rabbits in each group, and they were sacrificed 4, 8, and 12 weeks after the surgery. They were performed with general observation, X-ray photography, and histological and biomechanical examinations. According to the Lane-Sandhu bone defect repair tissue X-ray and histological scoring standard, the effect of bone defect repair was evaluated. It was found that the actual pore structure of the scaffold prepared by the SLM process was consistent with the theoretical design. The observation under TEM showed that rhBMP-2/PLA SRNs were approximately round, with an average particle size of 835 nm, and its encapsulation efficiency and drug loading rate were $89.02 \pm 5.14\%$ and $0.033 \pm 0.004\%$, respectively. The rhBMP-2/PLA SRNs and BPTAS had no statistically obvious increase in the number of cells after cell treatment compared with the control group ($P > 0.05$). At 12 weeks postoperatively, the stent bone tissue growing distance (SBTGD) in the SRN group was longer than that in the A1000 group ($P < 0.01$), and that in the A1000 group was better in contrast to the A800, A1200, and A1500 groups ($P < 0.01$). The Lane-Sandhu X-ray score of the SRN group was better than other groups ($P < 0.05$). It suggested that 3DP-BPTAS and rhBMP-2/PLA SRNs could repair the bone defects, and rhBMP-2/PLA SRNs were more conducive to the formation of new bone tissue.

DOI: <http://dx.doi.org/10.14715/cmb/2022.68.3.11>

Copyright: © 2022 by the C.M.B. Association. All rights reserved



Introduction

Bone defects are one of the common complications of orthopedic surgery caused by infections, tumors, congenital bone diseases, and other factors. In recent years, new cases of bone defects have been reported to be an obvious upward trend due to the aging of the population and the continuous development of transportation. Some bone defects will repair by themselves, but it is difficult for bone defects with a volume of more than $6 * 6 * 10$ to heal completely by themselves (1). Autologous bone transplantation is the "gold standard" for bone defects clinical repair, but it has limited sources, causing secondary damage when

it is taken, and increasing patient suffering (2). In addition, the use of allogeneic bone transplantation also has the risk of immune rejection reaction and infectious disease (3). Artificial bone has the advantages of a wide range of sources, can be sterilized and alleviates the pain of bone removal in patients, so it has a good application prospect in the treatment of bone defects (4).

Titanium and its alloys have the characteristics of good biocompatibility, mechanical properties and stability, but titanium is biologically inert, and the worn or polished titanium loses the ability of osseointegration (5). In addition, the elastic modulus

*Corresponding author. E-mail: www20160812@163.com
Cellular and Molecular Biology, 2022, 68(3): 86-95

of titanium and its alloys is much higher than that of normal human bone tissue, which is easy to cause stress shielding effect, leading to the phenomenon of endophytic prosthesis loosening (6). Making titanium and its alloys into a porous structure closer to human bone tissue can significantly reduce its elastic modulus, reduce the generation of stress shielding effect, and is more conducive to promoting bone tissue growth (7). The void size, porosity, and shape of the porous structure material have a significant impact on the bone ingrowth effect in the scaffold (8). However, traditional methods can't precisely control the parameters such as the pore size and shape of the porous structure (9). Three-dimensional (3D) printing technology can achieve precise control of the pore structure of porous titanium and its alloys (10). Recombinant human bone morphogenetic protein 2 (rhBMP-2) is the cytokine with the strongest osteogenesis effect. It can be used to promote fracture repair, but it has the disadvantages of being easily diluted by body fluids and short half-life in inducing bone formation in the body, which reduces the osteogenesis ability (11). Using polymer materials to embed cytokines for the slow release can make the drug release slowly and maintain the local effective drug stimulation concentration (12).

In summary, the porous titanium alloy scaffold and rhBMP-2 play significant roles in promoting bone repair, but they still have certain shortcomings. In bone defect modification, which of the porous titanium alloy scaffold and rhBMP-2 nanomaterials is more advantageous is not yet known. Therefore, selective laser melting technology (SLM) and double emulsion solvent volatilization was adopted in this study to prepare porous titanium alloy scaffolds and rhBMP-2/PLA sustained-release microspheres bone repair materials. A bone defect animal model was established, and the two repair materials were applied to the treatment of bone defect to explore the effect of 3D printing bioactive porous titanium alloy scaffold and rhBMP-2/PLA slow-release microspheres in the treatment of bone defect, which can provide a basis for reference for bone defect treatment.

Materials and Methods

Preparation of bioactive porous titanium alloy scaffolds (BPTAS)

UG software (Siemens PLM Software) was used to design BPTAS with pore diameters of 800 μm , 1000 μm , 1200 μm , and 1500 μm . Titanium alloy powder

with a diameter of 15 ~ 53 μm (Feierkang Rapid Manufacturing Technology Co., Ltd.) was used as raw material to prepare the BPTAS using a selective laser melting 3D printing equipment (Hunan Huashu High-tech Co., Ltd.) under the conditions of 200 W laser power, 200 mm/s scanning speed, and 120 μm shadow distance. The prepared samples were treated at 1300°C for 1 hour, cooled naturally under argon protection, cleaned with an ultrasonic cleaner, and dried in an oven for later use.

Preparation of rhBMP-2/PLA-loaded SRNs

A certain amount of rhBMP-2 powder (Shanghai Ruibang Biomaterials Co., Ltd.) was dissolved in 1 mL of double-distilled water and stirred and mixed as the water phase. The poly lactic acid (PLA) (Jinan Daigang Bioengineering Co., Ltd.) was dissolved in the mixture of 4 mL of dichloromethane and 1 mL of acetone, which was undertaken as the oil phase. The water phase was slowly dipped into the oil phase under stirring conditions and stirred with an ultrasonic disperser (Nanjing Shunma Instrument Equipment Co., Ltd.) for 1 min at a power of 100 W at 4°C to form colostrum. It was slowly put to 1% polyvinyl alcohol (PVA) (Tianjin Komiou Chemical Reagent Co., Ltd.) solution, and stirred with a magnetic stirrer (Tianjin Komiou Chemical Reagent Co., Ltd.) at 4°C at 400rp/min for 5 hours. The precipitate was collected by centrifugation at 12,000 rp/min for 20 minutes and washed with double distilled water 3 times. After freeze-drying, it was irradiated with 3000Gy⁶⁰Co for 30 minutes to obtain rhBMP-2/PLA-loaded SRNs. The specific preparation process was shown in Figure 1.

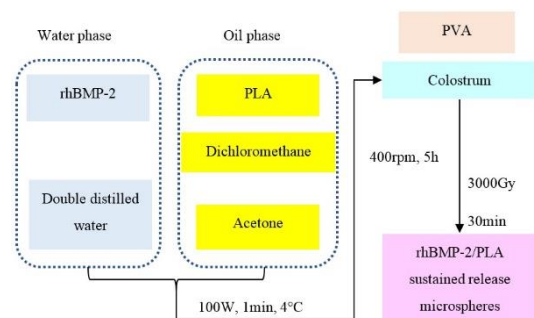


Figure 1. The preparation process of rhBMP-2/PLA-loaded SRNs.

Characterization analysis of bone repair materials

A scanning electron microscope (SEM) (Hitachi S-3400N, Japan) was used to observe the morphology of BPTAS and rhBMP-2/PLA-loaded SRNs. The actual aperture of the BPTAS was measured by an electron microscope system, 5 samples of each specification were randomly tested, and the average value and relative error (Re) were calculated. The calculation method of Re was $Re = \left[\frac{|A - D|}{D} \right] \times 100\%$, where A referred to the average value of the measured aperture and D represented the design aperture value. A laser particle size analyzer (Nano ZS, Malvern Instruments Co., Ltd., UK) was adopted to detect the particle size of rhBMP-2/PLA-loaded SRNs.

Determination of drug loading, encapsulation rate, and release amount of rhBMP-2/PLA-loaded SRNs

According to the method given by Lyu et al. (2020) [13], the prepared SRNs were added to 1 mL of 0.1 mol/L sodium hydroxide (NaOH) solution containing 50 g/L lauryl sodium sulfate (SDS), incubated at 37°C for 24 hours, and then cooled to room temperature. The human rhBMP-2 enzyme-linked immunosorbent assay (ELISA) kit was adopted to detect the optical density (OD) at 450 nm. The concentration of rhBMP-2 in SRNs was calculated according to the standard curve, and the drug loading (DL) and encapsulation rate (ER) of rhBMP-2 in SRNs were calculated with $DL = C/M_1 \times 100\%$ and $ER = C/M_2 \times 100\%$, respectively. In the equations, C was the content of rhBMP-2 in SRNs, M_1 referred to the weight of SRNs; and M_2 represented the weight of rhBMP-2 added when the microcapsules were prepared.

The SRNs were put into 5 mL of 0.01 M/L Phosphate Buffer Saline (PBS) buffer (pH = 7.3), and incubated with shaking at 37°C. 1 mL of supernatant was taken on the 1st, 3rd, 5th, 7th, 9th, 11th, 13th, 15th, 17th, and 19th day to detect the OD at 450 nm using the human rhBMP-2 ELISA kit. After the supernatant was removed, it was added with an equal volume of PBS buffer (pH = 7.3) to calculate the cumulative release of rhBMP-2 in SRNs.

Effects of bone repair materials on BMSCs

The SRNs were added to low-sugar Dulbecco's modified eagle medium (DMEM) (10% fetal bovine serum (FBS)) and incubated at 37°C for 24 hours. The

concentration of BMSCs cells with good growth status was adjusted to 5×10^4 cells/mL with DMEM, and then 100 μ L was added to 96-well plates and cultured for 24 hours. The cell culture medium was aspirated, and the SRNs supernatant after 24 hours of treatment was added. For the control group, only DMEM was added. The cells were cultured at 37°C for 24h, 36h, 48h, 60h, and 72h, and the OD value of the sample was detected by the MTT method.

After trypsinization of BMSCs cells in good growing conditions, the cells were washed twice with PBS. The concentration of BMSCs cells with good growth status was adjusted to 3×10^5 cells/mL by using DMEM, and 100 μ L was put into 96-well plates and cultured for 24 hours. The cell suspension was co-cultured with BPTAS and incubated at 37°C for 24h, 36h, 48h, 60h, and 72h, and the OD value of the sample was detected by the MTT method.

The porous titanium alloy scaffolds and slow-release microspheres which were cultured for 7 days were fixed with 4% paraformaldehyde; after rinsing with 0.01M phosphate buffer solution 3 times, they were rinsed with distilled water 3 times to avoid residual salt crystals on the surface of the microsphere holder after drying and affecting the observation results. The vacuum drying was performed to remove more than water, and an appropriate amount of dried sample was taken and placed on the copper plate, which was coated evenly. It should sputter gold with Eiko IB-5 ion plating instrument under vacuum, and observe the surface morphology of porous titanium alloy scaffold and slow-release microspheres after cell attachment and growth by SEM.

Source and grouping of experimental animals

63 healthy male rabbits, weighing 2.5 - 3.5kg, were selected and housed in a clean experimental animal room in a conventional single cage, with a room temperature of 25°C and relative humidity of about 55%, under 12 hours of light for free drinking and eating. All rabbits were randomly rolled into a control group (no treatment), a model group (the femoral condyle defect model), an A800 group (model + 800 μ m of BPTAS), and an A1000 group (model + 1000 μ m of BPTAS), an A1200 group (model + 1200 μ m of BPTAS), an A1500 group (model + 1500 μ m of BPTAS), and an SNR group (model + rhBMP-2/PLA SRNs), with 9 rabbits in each group. All animal

procedures in this experiment were approved by the Experimental Animal Management Committee, and the experimental methods were carried out in accordance with the approved guidelines.

Model establishment and treatment of bone defects

Before modeling, all animals fasted for 12 hours, and 20% urethane solution was used as an anesthetic to be injected intraperitoneally at 5 mL/kg. After the anesthesia was satisfied, 800,000 U/head of penicillin was injected intramuscularly. The hair was shaved and the skin in the area was prepared, and the operation area was routinely disinfected with iodophor. With reference to the method of Lee et al. (2019) [14], a longitudinal incision was made on the lateral condyle of the right femur of the rabbit. The size of the incision was about 3 cm, which fully exposed the raised bony surface and cortical bone of the lateral femoral condyle. A 2 mm grinder was adopted to drill the holes for positioning, and a 6 mm grinder was adopted to drill 9 mm deep bone defects holes. The wound was washed with saline and hydrogen peroxide, and the fascia and skin were sutured with 3-0 nylon sutures, and sterile gauze was covered and bandaged with iodophor again after the operation was sterilized. All animals were marked with gentian violet solution after surgery, and all animals were moved to cages and then fed in single cages. On the second day after surgery, 800,000 U/piece of penicillin was injected intramuscularly for 3 days once a day, and the dressing was changed in the operation area every 2 days.

The specific treatment methods for different groups were as follows. After the animals had established bone defects area and disinfected, the disinfected 800 μm , 1000 μm , 1200 μm , and 1500 μm BPTAS and rhBMP-2/PLA-loaded SRNs (containing 2.5 μg of rhBMP-2) were implanted in the defect area, which was disinfected, sutured and again disinfected and bandaged. In addition, the corresponding postoperative treatment was carried out.

Observation indicators and methods

The mentality, diet, activity, and wound healing of different groups of rabbits were observed after surgery. X-ray examination was performed on the defect site 12 weeks after the operation to observe the healing of bone defects in different groups of animals.

According to the Lane-Sandhu bone defects repair tissue X-ray scoring standard [15], the effect of bone defect repair in different groups of animals was evaluated. The rabbits were euthanized at 4 weeks, 8 weeks, and 12 weeks after the surgery. The middle section of the bone defect was taken, tissue sections were made, and hematoxylin-eosin staining was performed for observation. It should refer to Lane-Sandhu histological scoring standard for evaluation [16], the higher the score, the more obvious the repair effect. The scoring was performed by a double-blind method, with the associate chief physician of the pathology department and above-qualified physicians for scoring. The HE-stained images were collected and the length of bone tissue was measured by the slice browsing software.

Statistical analysis

SPSS 19.0 was used for data statistics and analysis. Measurements were expressed in the form of mean \pm standard deviation ($\bar{x} \pm s$). Data differences among groups were analyzed by one-way analysis of variance, and $P < 0.05$ indicated that the differences were statistically significant.

Results and discussion

Characterization and analysis of bone repair materials

The SEM images of prepared BPTAS with different pore sizes were observed, and the observation results were shown in Figure 2. The pores of different specifications of scaffolds were evenly distributed and showed good penetration (Figure 2A). The pores of the 800 μm and 1000 μm scaffolds were irregular in shape (Figure 2B and Figure 2C), and the pores of the 1200 μm and 1500 μm scaffolds were rhomboid (Figure 2D and Figure 2E). The rhBMP-2/PLA-loaded SRNs showed a spherical shape, uniform size distribution, and smooth surface under SEM (Figure 2F).

The pore size test results and error rates of different specifications of BPTAS were statistically analyzed, and the results were shown in Figure 3. The pore sizes of the 800 μm , 1000 μm , 1200 μm , and 1500 μm scaffolds were $803 \pm 61 \mu\text{m}$, $998 \pm 55 \mu\text{m}$, $1156 \pm 70 \mu\text{m}$, and $1484 \pm 43 \mu\text{m}$, respectively (Figure 3A), and the corresponding relative error rates were 3.75%, 2.00%, 10.67%, and 36.67%, respectively (Figure

3A). The particle size distribution range of rhBMP-2/PLA-loaded SRNs was 692.44 nm - 981.63 nm, and the average particle size was 835 nm, as illustrated in Figure 3B.

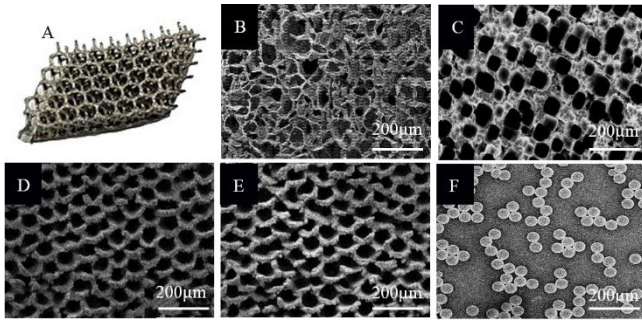


Figure 2. Morphology of bone repair material. Note: Figures A ~ F showed the appearance of BPTAS; SEM image of 800 μmscaffolds, SEM image of 1000 μmscaffolds, SEM image of 1200 μmscaffolds, SEM image of 1500 μmscaffolds, and SEM image of rhBMP-2/PLA-loaded SRNs, respectively.

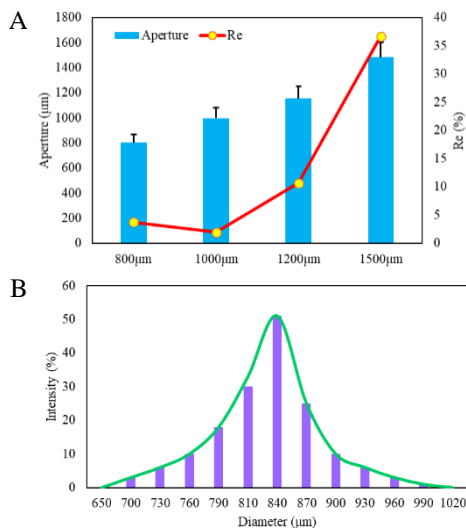


Figure 3. Analysis of pore size of bone repair materials. Note: Figure A showed the different specifications of BPTAS aperture and relative error rate, and Figure B was the diameter distribution diagram of BrhBMP-2/PLA-loaded SRNs.

Analysis of DL, ER, and release test results of rhBMP-2/PLA-loaded SRNs

At the maximum absorption wavelength of 450 nm, as the concentration of rhBMP-2 continued to increase, the OD of the microspheres showed an upward trend (as given in Figure 4). According to the linear relationship between the OD of rhBMP-2 and the corresponding concentration, the corresponding ER and DL were calculated. The ER of rhBMP-2/PLA-loaded SRNs was $89.02 \pm 5.14\%$, and the DL

was $0.033 \pm 0.004\%$. The cumulative release of rhBMP-2/PLA SRNs increased first and then stabilized. The release of rhBMP-2 was 9.74% on the 1st day, and stable on the 7th day, and the cumulative release rate of rhBMP-2 was 78.16% on the 19th day (as illustrated in Figure 5).

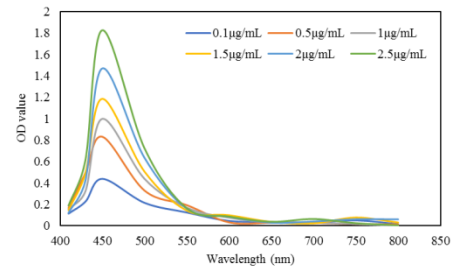


Figure 4. UV-Vis absorption spectra of SRNs at different concentrations.

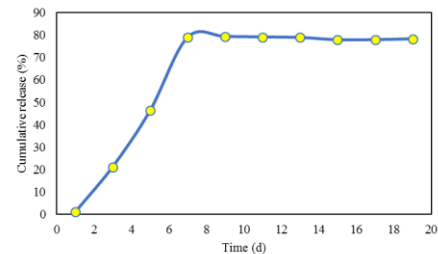


Figure 5. The cumulative release of rhBMP-2/PLA-loaded SRNs in different time periods.

Effects of bone repair materials on the proliferation of BMSCs

The effect of different specifications of BPTAS on the proliferation of BMSCs was shown in Figure 6. With the extension of time, the OD values of cells co-cultured with different specifications of scaffolds and BMSCs showed a trend of first increasing and then decreasing, and there was no statistical difference in the OD values of BPTAS with different pore sizes ($P > 0.05$). The OD values of BMSC cells in the control group at different periods were not statistically obvious compared with different specifications of BPTAS ($P > 0.05$). The OD values of BMSCs in the control group at different periods were not statistically observable compared with BMSCs treated with SRNs ($P > 0.05$).

The porous titanium alloy scaffolds of different specifications were co-cultured with BMSCs for 7 days and then scanned by electron microscope (Figures 7A ~ 7D). BMSCs cells resemble a spindle shape, begin to stretch, and initially protrude

pseudopodia. BMSCs adhered to porous titanium alloy scaffolds of different specifications, and both protrude filopodia and lamellipodia. Each group of cells adhered well to the surface of the substrate. The rhBMP-2/PLA sustained-release microspheres were co-cultured with BMSCs for 7 days and then scanned by SEM (Figures 7A ~ 7E). The BMSCs cells stretched into a long spindle shape and protruded pseudopods to adhere around the sustained-release microspheres, and the cell division and proliferation were normal. It showed that BMSCs cells gradually expanded and grew into the pores of the porous titanium alloy scaffold and slow-release microspheres.

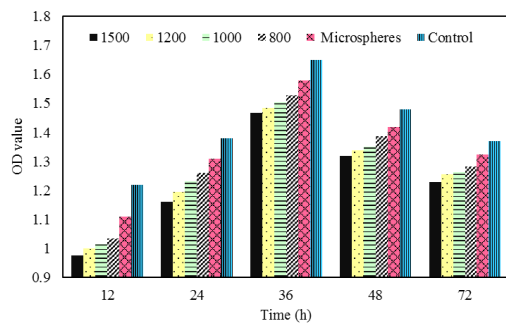


Figure 6. Effects of bone repair materials on the proliferation of BMSCs.

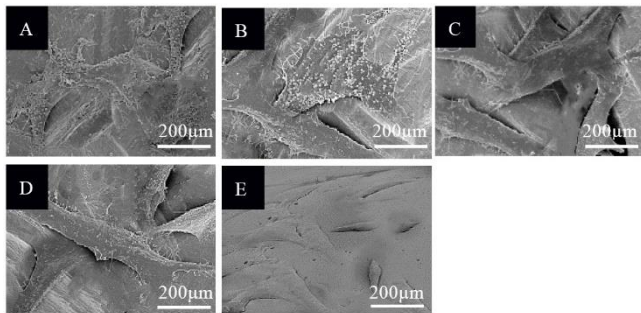


Figure 7. The morphology of nanomaterials and BMSCs were co-cultured for 7 days. (A: co-cultivation of 800 μ m porous titanium alloy scaffold and BMSCs; B: co-cultivation of 1000 μ m porous titanium alloy scaffold and BMSCs; C: co-cultivation of 1200 μ m porous titanium alloy scaffold and BMSCs; D: co-cultivation of 1500 μ m porous titanium alloy scaffold and BMSCs; and E: co-cultivation of rhBMP-2/PLA sustained-release microspheres and BMSCs)

Analysis of X-ray results of different groups

The cortical bone of the control group had good continuity and the bone marrow cavity had good penetration (Figure 8A). X-rays of the model group showed that more calluses were formed at both ends of bone defects, and there were obvious defects

(Figure 8B). The X-ray examination results of the BPTAS and SRNs group at 12 weeks after surgery showed that the material and the host bone were healed, and the morphology returned to normal (Figure 8C and Figure 8D).



Figure 8. X-ray examination results of 12 weeks after operation in different groups. Note: Figures A ~ D showed the X-ray examination results of the control group, model group, BPTAS A1000 group, and rhBMP-2/PLA-loaded SRNs group, respectively.

The X-ray scores of Lane-Sandhu bone defects repair tissues in different groups were compared, and the results were illustrated in Figure 9. The Lane-Sandhu score of the A1000 group was higher than that of the model group at 4 and 8 weeks after surgery ($P < 0.05$); The Lane-Sandhu scores of the SRNs group and the control group were much higher than the model group at 4 and 8 weeks after surgery ($P < 0.01$), and the Lane-Sandhu scores of the SRNs group and the control group were higher greater than the model group at 12 weeks after surgery ($P < 0.001$).

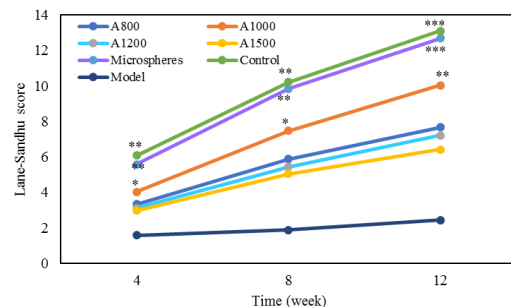


Figure 9. Lane-Sandhu score results of different groups. Note: * and ** suggested that the difference in contrast to the model group was statistically obvious ($P < 0.05$) and extremely statistically obvious ($P < 0.01$), respectively. *** indicated $P < 0.001$ compared with the model group.

Pathological observation of tissue slices in different groups of bone defects

HE staining was performed on the tissues of the bone defect at 12 weeks postoperatively in different groups, and the results were analyzed, as shown in Figure 10. Obvious bone defect areas can be seen in the model group. The bone tissue in the control group was complete. The bone defect of the A1000, A1200, and A1500 groups in the A800 group had completed bone connection, and the formation of cortical bone can be observed. The recanalization of the medullary cavity was seen in the A1000 group, and the stent recanalization was not completed in the A800 group, A1200 group, and A1500 group. In the nano-microsphere group, there was no inflammatory cell or inflammatory response caused by the microsphere carrier. The bone defect had completed bone connection, the formation of the bone cortex could be observed, and the recanalization of the medullary cavity was completed.

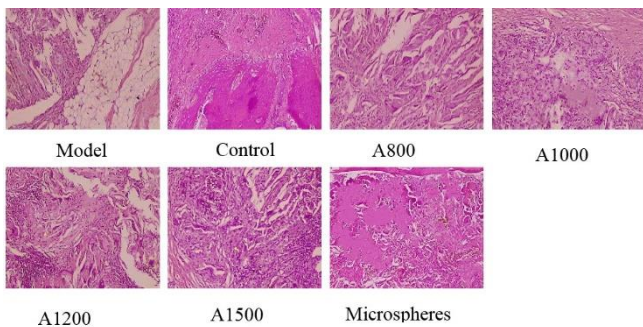


Figure 10. HE staining of tissues of bone defects in different groups ($\times 200$).

The Lane-Sandhu histological scoring results of different groups were further analyzed, and the results were shown in Figure 11. The Lane-Sandhu histological score of the control group was 10.98 ± 1.27 , and that in the model group was 1.92 ± 0.21 . The Lane-Sandhu histological scores of the A800 group, A1000 group, A1200 group, and A1500 group were 3.17 ± 0.33 , 7.19 ± 0.74 , 6.05 ± 0.63 , and 5.54 ± 0.57 , respectively. The Lane-Sandhu histological score of the nanosphere group was 10.27 ± 1.06 . The Lane-Sandhu histological score of the model group was significantly lower than that of the control group ($P < 0.001$), the score of the A1000 group was higher than that of the control group ($P < 0.05$), and compared with the control group, the Lane-Sandhu

histological score of the nanosphere group was significantly different ($P < 0.01$).

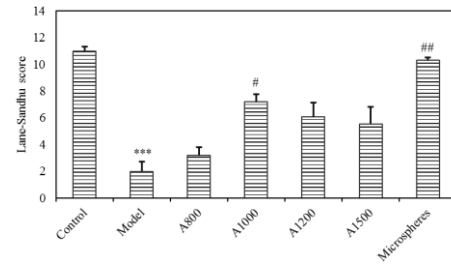


Figure 11. Comparison of Lane-Sandhu histological scores in different groups. (** indicated a significant difference compared with the model group ($P < 0.001$); # indicated a statistical difference compared with the control group ($P < 0.05$); and ## indicated a significant difference compared with the control group ($P < 0.01$)).

Comparison of results of general observation and growth of bone tissue

Except for the control group, animals in the other groups showed varying degrees of limb weakness and poor eating within 24 hours after surgery and showed mild claudication within one week after surgery. No limb fracture or paralysis was found in all experimental animals.

As illustrated in Figure 12, at 4 weeks postoperatively, the SBTGD in the A800 group and the SRNs group was greater than that in the A1000, A1200, and A1500 groups ($P < 0.05$). At 8 weeks, the SBTGD in the SRNs group was greater than that in the A1000 group ($P < 0.05$), and the SBTGD in the A1000 group was better than A800, A1200, and A1500 groups ($P < 0.05$). At 12 weeks, the SBTGD in the SRNs group was greater than that in the A1000 group ($P < 0.01$), and the SBTGD in the A1000 group was better than that in the A800, A1200, and A1500 groups ($P < 0.01$).

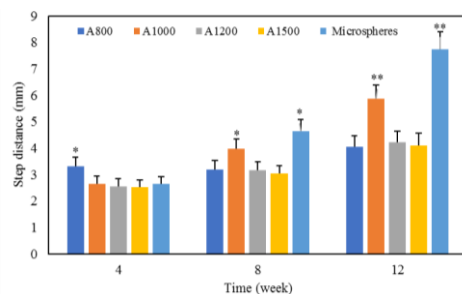


Figure 12. Growth distance of bone tissue in different groups. Note: * and ** suggested that the difference in contrast to the A1200 group was statistically obvious ($P < 0.05$) and extremely statistically obvious ($P < 0.01$), respectively.

The results of this study revealed that the pores of the 800 μm and 1000 μm scaffolds were irregular in shape, and the pores of the 1200 μm and 1500 μm scaffolds were rhomboid. Such results indicate that as the pore size increases, the pore shape of BPTAS is better controlled. The reason for the analysis may be that under low pore size, a large number of incompletely melted titanium powder particles adhere to the surface of the stent, which is bonded to the rod after SLM treatment, resulting in the irregular shape of the pores on the surface of the stent (17,18). Current research results show that porous scaffolds can increase the contact area between bone and implant (19), and promote bone ingrowth and osseointegration (20). Osteogenic polylactic acid (PLA) is a degradable polymer biomaterial with good biocompatibility and absorbability (21). It has been used in surgical sutures, and oral and ophthalmic implant materials (22). The ER and DL can reflect the degree of drug encapsulation (23). The drug release of microspheres is mainly through the desorption and diffusion of the drug on the surface of the carrier material. With the gradual degradation and dissolution of the carrier material, until it is completely degraded, the drug is completely released (24). In this study, it was combined with rhBMP-2 to prepare rhBMP-2/PLA-loaded SRNs with an average particle size of 835 nm. The ER and DL were $89.02 \pm 5.14\%$ and $0.033 \pm 0.004\%$, respectively. The release of rhBMP-2 was stable after the 7th day, and the cumulative release rate of rhBMP-2 was 78.16% on the 19th day. It shows that rhBMP-2/PLA-loaded SRNs have an obvious slow-release effect.

The results of this study found that at 12 weeks, the SBTGD in the SRNs group was greater than that in the A1000 group ($P < 0.01$), and the SBTGD in the A1000 group was better than that in the A800, A1200, and A1500 groups ($P < 0.01$). The Lane-Sandhu score was greatly higher than the model group ($P < 0.001$). These results indicate that BPTAS and rhBMP-2/PLA-loaded SRNs have a certain ability to repair bone defects, and rhBMP-2/PLA-loaded SRNs have significant advantages in the formation of new bone tissue. The reason may be that rhBMP-2 plays an important role. rhBMP-2 is an essential component of the signal pathway that controls bone defect repair (25-26).

Conclusions

In this study, different methods were used to prepare active BPTAS and rhBMP-2/PLA-loaded SRNs and applied them in the treatment of bone defects. The results showed that 3DP-BPTAS and rhBMP-2/PLA-loaded SRNs both showed better repair ability on bone defects. Compared with the two treatment effects, rhBMP-2/PLA-loaded SRNs had advantages. However, this study did not examine the biomechanical properties of bone tissue after different bone repair materials, and future work would further verify the difference in biomechanical properties of the two bone repair materials. In summary, rhBMP-2/PLA-loaded SRNs were more effective in the treatment of bone defects, which provided a theoretical basis for the treatment of bone defects.

Acknowledgments

The research is supported by: Hospital General Project of Affiliated Hospital of Yan'an University, Research on key technology of tissue regeneration of 3D printing bioactive porous titanium alloy scaffolds in the treatment of bone defects (No. 2021PT-04); Yan'an Science and Technology Planning Project, Key R & D projects, Research on key technology of tissue regeneration of 3D printing bioactive porous titanium alloy scaffolds in the treatment of bone defects (No. SL2019ZCSZ-006).

Interest conflict

The authors declare that they have no conflict of interest.

References

1. Oryan A, Alidadi S. Reconstruction of radial bone defect in rat by calcium silicate biomaterials. *Life Sci* 2018; 201: 45-53.
2. Srouji S, Blumenfeld I, Rachmiel A, Livne E. Bone defect repair in rat tibia by TGF-beta1 and IGF-1 released from hydrogel scaffold. *Cell Tissue Bank* 2004; 5(4): 223-230.
3. Oryan A, Alidadi S, Bigham-Sadegh A, Moshiri A. Healing potentials of polymethylmethacrylate bone cement combined with platelet gel in the critical-sized radial bone defect of rats. *PLoS One* 2018; 13(4): e0194751.
4. Machavariani A, Menabde G, Zurmukhtashvili M. Guided regeneration of jaw bone defects with combination of osteoplastic materials and stem cells. *Georgian Med News* 2019; (290): 131-135.

5. Kaur M, Singh K. Review on titanium and titanium based alloys as biomaterials for orthopaedic applications. *Mater Sci Eng C Mater Biol Appl* 2019; 102: 844-862.
6. Ottria L, Lauritano D, Andreasi Bassi M, Palmieri A, Candotto V, Tagliabue A, Tettamanti L. Mechanical, chemical and biological aspects of titanium and titanium alloys in implant dentistry. *J Biol Regul Homeost Agents* 2018; 32(2 Suppl. 1): 81-90.
7. Koizumi H, Takeuchi Y, Imai H, Kawai T, Yoneyama T. Application of titanium and titanium alloys to fixed dental prostheses. *J Prosthodont Res* 2019; 63(3): 266-270.
8. Zhang C, Zhang L, Liu L, Lv L, Gao L, Liu N, Wang X, Ye J. Mechanical behavior of a titanium alloy scaffold mimicking trabecular structure. *J Orthop Surg Res* 2020; 15(1): 40.
9. Zhan X, Li S, Cui Y, Tao A, Wang C, Li H, Zhang L, Yu H, Jiang J, Li C. Comparison of the osteoblastic activity of low elastic modulus Ti-24Nb-4Zr-8Sn alloy and pure titanium modified by physical and chemical methods. *Mater Sci Eng C Mater Biol Appl* 2020; 113: 111018.
10. Takeuchi Y, Tanaka M, Tanaka J, Kamimoto A, Furuchi M, Imai H. Fabrication systems for restorations and fixed dental prostheses made of titanium and titanium alloys. *J Prosthodont Res* 2020; 64(1): 1-5.
11. Han SH, Jung SH, Lee JH. Preparation of beta-tricalcium phosphate microsphere-hyaluronic acid-based powder gel composite as a carrier for rhBMP-2 injection and evaluation using long bone segmental defect model. *J Biomater Sci Polym Ed* 2019; 30(8): 679-693.
12. Alraei K, Sharqawi J, Harcher S, Ghita I. Efficacy of the Combination of rhBMP-2 with Bone Marrow Aspirate Concentrate in Mandibular Defect Reconstruction after a Pindborg Tumor Resection. *Case Rep Dent* 2020; 2020: 8281741.
13. Lyu HZ, Lee JH. The efficacy of rhBMP-2 loaded hydrogel composite on bone formation around dental implants in mandible bone defects of minipigs. *Biomater Res* 2020; 24: 5.
14. Lee YC, Chan YH, Hsieh SC, Lew WZ, Feng SW. Comparing the Osteogenic Potentials and Bone Regeneration Capacities of Bone Marrow and Dental Pulp Mesenchymal Stem Cells in a Rabbit Calvarial Bone Defect Model. *Int J Mol Sci* 2019; 20(20): 5015.
15. Klüter T, Hassan R, Rasch A, Naujokat H, Wang F, Behrendt P, Lippross S, Gerdesmeyer L, Eglin D, Seekamp A, Fuchs S. An Ex Vivo Bone Defect Model to Evaluate Bone Substitutes and Associated Bone Regeneration Processes. *Tissue Eng Part C Methods* 2020; 26(1): 56-65.
16. Helbig L, Guehring T, Titze N, Nurjadi D, Sonntag R, Armbruster J, Wildemann B, Schmidmaier G, Gruetzner AP, Freischmidt H. A new sequential animal model for infection-related non-unions with segmental bone defect. *BMC Musculoskelet Disord* 2020; 21(1): 329.
17. Tretto PHW, Dos Santos MBF, Spazzin AO, Pereira GKR, Bacchi A. Assessment of stress/strain in dental implants and abutments of alternative materials compared to conventional titanium alloy-3D non-linear finite element analysis. *Comput Methods Biomech Biomed Engin* 2020; 23(8): 372-383.
18. Pan Y, Lin Y, Jiang L, Lin H, Xu C, Lin D, Cheng H. Removal of dental alloys and titanium attenuates trace metals and biological effects on liver and kidney. *Chemosphere* 2020; 243: 125205.
19. Srncic R, Divin R, Škorič M, Snášil R, Krbec M, Nečas A. Use of the Peptigel with Nanofibres in the Bone Defects Healing. *Acta Chir Orthop Traumatol Cech* 2018; 85(5): 359-365.
20. Balaguer T, Fellah BH, Boukhechba F, Traverson M, Mouska X, Ambrosetti D, Dadone B, Michiels JF, Amri EZ, Trojani C, Bouler JM, Gauthier O, Rochet N. Combination of blood and biphasic calcium phosphate microparticles for the reconstruction of large bone defects in dog: A pilot study. *J Biomed Mater Res A* 2018; 106(7): 1842-1850.
21. Han SH, Cha M, Jin YZ, Lee KM, Lee JH. BMP-2 and hMSC dual delivery onto 3D printed PLA-Biogel scaffold for critical-size bone defect regeneration in rabbit tibia. *Biomed Mater* 2020; 16(1): 015019.
22. Zhang HY, Jiang HB, Kim JE, Zhang S, Kim KM, Kwon JS. Bioresorbable magnesium-reinforced PLA membrane for guided bone/tissue regeneration. *J Mech Behav Biomed Mater* 2020; 112: 104061.
23. Strong ME, Richards JR, Torres M, Beck CM, La Belle JT. Faradaic electrochemical impedance spectroscopy for enhanced analyte detection in diagnostics. *Biosens Bioelectron* 2021; 177: 112949.
24. Ma F, Yan J, Sun L, Chen Y. Electrochemical impedance spectroscopy for quantization of matrix Metalloproteinase-14 based on peptides inhibiting its homodimerization and heterodimerization. *Talanta* 2019; 205: 120142.
25. Darvishi E, Kahrizi D, Arkan E, Hosseinabadi S, Nematpour N. Preparation of bio-nano bandage from quince seed mucilage/ZnO nanoparticles

- and its application for the treatment of burn. *J Mol Liq* 2021;339:116598. doi: 10.1016/j.molliq.2021.116598.
26. Senatov F, Amanbek G, Orlova P, Bartov M, Grunina T, Kolesnikov E, Maksimkin A, Kaloshkin S, Poponova M, Nikitin K, Krivozubov M, Strukova N, Manskikh V, Anisimova N, Kiselevskiy M, Scholz R, Knyazeva M, Walther F, Lunin V, Gromov A, Karyagina A. Biomimetic UHMWPE/HA scaffolds with rhBMP-2 and erythropoietin for reconstructive surgery. *Mater Sci Eng C Mater Biol Appl* 2020; 111: 110750.